Progress in Oceanography 151 (2017) 261–274

Contents lists available at ScienceDirect

Progress in Oceanography

journal homepage: www.elsevier.com/locate/pocean

Phosphorus dynamics in biogeochemically distinct regions of the southeast subtropical Pacific Ocean

Solange Duhamel [a,b,*], Karin M. Björkman [b], Daniel J. Repeta [c], David M. Karl [b]

[a] Lamont-Doherty Earth Observatory, Division of Biology and Paleo Environment, PO Box 1000, 61 Route 9W, Palisades, NY 10964, USA
[b] Daniel K. Inouye Center for Microbial Oceanography: Research and Education (C-MORE), University of Hawaii, C-MORE Hale, 1950 East West Road, Honolulu, HI 96822, USA
[c] Departmentof Chemistry and Geochemistry, Woods Hole Oceanographic Institution, Woods Hole, MA 02543, USA

ARTICLE INFO

Article history:
Received 28 December 2015
Received in revised form 27 December 2016
Accepted 27 December 2016
Available online 29 December 2016

Keywords:
Phosphorus dynamics
Microbes
Stocks
Fluxes
Southeast subtropical Pacific Ocean

ABSTRACT

The southeast subtropical Pacific Ocean was sampled along a zonal transect between the coasts of Chile and Easter Island. This remote area of the world's ocean presents strong gradients in physical (e.g., temperature, density and light), chemical (e.g., salinity and nutrient concentrations) and microbiological (e.g., cell abundances, biomass and specific growth rates) properties. The goal of this study was to describe the phosphorus (P) dynamics in three main ecosystems along this transect: the upwelling regime off the northern Chilean coast, the oligotrophic area associated with the southeast subtropical Pacific gyre and the transitional area in between these two biomes. We found that inorganic phosphate (Pi) concentrations were high and turnover times were long (>210 nmol l^{-1} and >31 d, respectively) in the upper water column, along the entire transect. Pi uptake rates in the gyre were low (euphotic layer integrated rates were 0.26 mmol m^{-2} d^{-1} in the gyre and 1.28 mmol m^{-2} d^{-1} in the upwelling region), yet not only driven by decreases in particle mass or cell abundance (particulate P- and cell- normalized Pi uptake rates in the euphotic layer were ~1–4 times and ~3–15 times lower in the gyre than in the upwelling, respectively). However these Pi uptake rates were at or near the maximum Pi uptake velocity (i.e., uptake rates in Pi amended samples were not significantly different from those at ambient concentration: 1.5 and 23.7 nmol l^{-1} d^{-1} at 50% PAR in the gyre and upwelling, respectively). Despite the apparent Pi replete conditions, selected dissolved organic P (DOP) compounds were readily hydrolyzed. Nucleotides were the most bioavailable of the DOP substrates tested. Microbes actively assimilated adenosine-5′-triphosphate (ATP) leading to Pi and adenosine incorporation as well as Pi release to the environment. The southeast subtropical Pacific Ocean is a Pi-sufficient environment, yet DOP hydrolytic processes are maintained and contribute to P-cycling across the wide range of environmental conditions present in this ecosystem.

1. Introduction

The biogeochemical cycling of phosphorus (P) in the ocean is not well characterized despite its importance as an essential nutrient for ocean productivity (Karl, 2000, 2014). Dissolved inorganic P (usually found in the form of free phosphate, Pi) is generally considered to be preferred for microbial nutrition, but its concentrations can be limiting in selected aquatic environments, particularly in oligotrophic marine habitats (Krom et al., 1991; Moutin et al., 2005; Dyhrman et al., 2007; Lomas et al., 2010). Dissolved organic P (DOP) concentrations often exceed those of Pi in surface waters and could serve as alternative sources of P for microbial nutrition (Paytan and McLaughlin, 2007; Karl and Björkman, 2015). Although much has been learned over the past decades about the chemical composition of marine DOP (Clark et al., 1998, 1999; Kolowith et al., 2001; Young and Ingall, 2010; Repeta et al., 2016) and its cycling (Björkman and Karl, 2003; Lomas et al., 2010; Duhamel et al., 2011; Ruttenberg and Dyhrman, 2012), much remains to be understood of its ecological role and the complex interactions with the marine microbial community. Only a minor fraction of the compound classes that comprise DOP can be characterized by available methods (e.g., ^{31}P NMR), limiting the prediction of the potential bioavailability of DOP (Karl and Björkman, 2015 and references therein). Yet, evidence based on changes in the stoichiometric composition of dissolved organic matter with depth showed that DOP is

* Corresponding author at: Lamont-Doherty Earth Observatory, Division of Biology and Paleo Environment, PO Box 1000, 61 Route 9W, Palisades, NY 10964, USA.
E-mail address: sduhamel@ldeo.columbia.edu (S. Duhamel).

http://dx.doi.org/10.1016/j.pocean.2016.12.007
0079-6611/

preferentially remineralized relative to organic carbon (C) and nitrogen (N), implying that it is mostly bioavailable (Clark et al., 1998; Karl et al., 2001; Kolowith et al., 2001). In addition, an increasing number of studies have shown that many microorganisms utilize DOP (see reviews in Dyhrman et al., 2007 and Karl and Björkman, 2015), suggesting that the pool of DOP is more dynamic than previously thought (Mather et al., 2008; Lomas et al., 2010; Duhamel et al., 2011).

The objective of the BiG RAPA (Biogeochemical Gradients: Role in Arranging Planktonic Assemblages) project was to investigate the impact of elemental nutrient ratios (C, N, P, silicon, iron) on marine productivity and microbial community composition in different trophic regimes in the southeast subtropical Pacific Ocean during the austral summer. A zonal transect at approximately 25°S between Chile and Easter Island was conducted in order to characterize the eutrophic layer associated with UP, the most productive and dynamic region, located in the upwelling area off the coast of Chile; GY, the most oligotrophic region located in the South Pacific subtropical gyre (SPSG) off the coast of Easter Island; and the transition zone (TR) in between, characterized by intermediary conditions to UP and GY (Fig. 1).

The southeast subtropical Pacific Ocean remains the most sparsely sampled region of the global ocean, in particular for biological and biogeochemical parameters (Claustre et al., 2008). Yet, the SPSG presents unique features that makes it a remarkable "end member" of oceanic environments; it is the largest subtropical anti-cyclonic gyre and has the lowest chlorophyll *a* (Chl) concentrations of the world's oceans, atmospheric iron flux and dinitrogen fixation rates are among the lowest and the SPSG has the "clearest" marine waters on Earth, allowing for deep penetration of visible sun light as well as ultraviolet radiation (Sverdrup et al., 1942; Claustre and Maritorena, 2003; Morel et al., 2007; Tedetti et al., 2007). Despite the low Chl and dissolved inorganic N concentrations previously reported from this area (nitrate was undetectable in the euphotic layer and only trace quantities (<20 nmol l^{-1}) of regenerated nitrogen—nitrite and ammonium—were detected; Raimbault et al., 2008), Pi concentrations remain above 100 nmol l^{-1} and do not appear to limit primary production (Bonnet et al., 2008; Moutin et al., 2008). However, published studies on the dynamics of P cycling in this part of the ocean is limited to the BIOSOPE 2004 field campaign in which standing stocks of dissolved and particulate pools of P were measured along with Pi uptake rates (Duhamel et al., 2007; Moutin et al., 2008; Duhamel and Moutin, 2009). Some information was also obtained on DOP fluxes and bioavailability by analysis of alkaline phosphatase activity (Duhamel et al., 2011). No information is currently available on the adaptation of microorganisms to ambient Pi and DOP concentrations.

The aim of the present study is to describe in greater detail the dynamics of P cycling in the euphotic layer within the three different regimes (UP, TR, GY) encountered in the southeast subtropical Pacific Ocean. Dissolved and particulate P-pool concentrations were analyzed and Pi and DOP turnover time were determined by radiotracer techniques. The contribution of different size fractions of the microbial communities to Pi and DOP uptake rate were also measured. The adaptation of microorganisms to ambient P concentrations was investigated by estimating their uptake kinetic characteristics. Finally, the bioavailability of selected DOP substrates to natural assemblages of microorganisms was evaluated.

2. Materials and methods

2.1. Sampling and hydrographic measurements

This work was conducted during the BiG RAPA cruise (18 November–14 December 2010). Sampling was performed on board the R/V Melville in the southeast subtropical Pacific Ocean between northern Chile and Easter Island (Fig. 1). Seven stations (S1; near Chile to S7; near Easter Island) were sampled either once on survey stations (S2, S3, S5 and S6; each occupied for one day) or two to three times on consecutive days at process stations (S1:

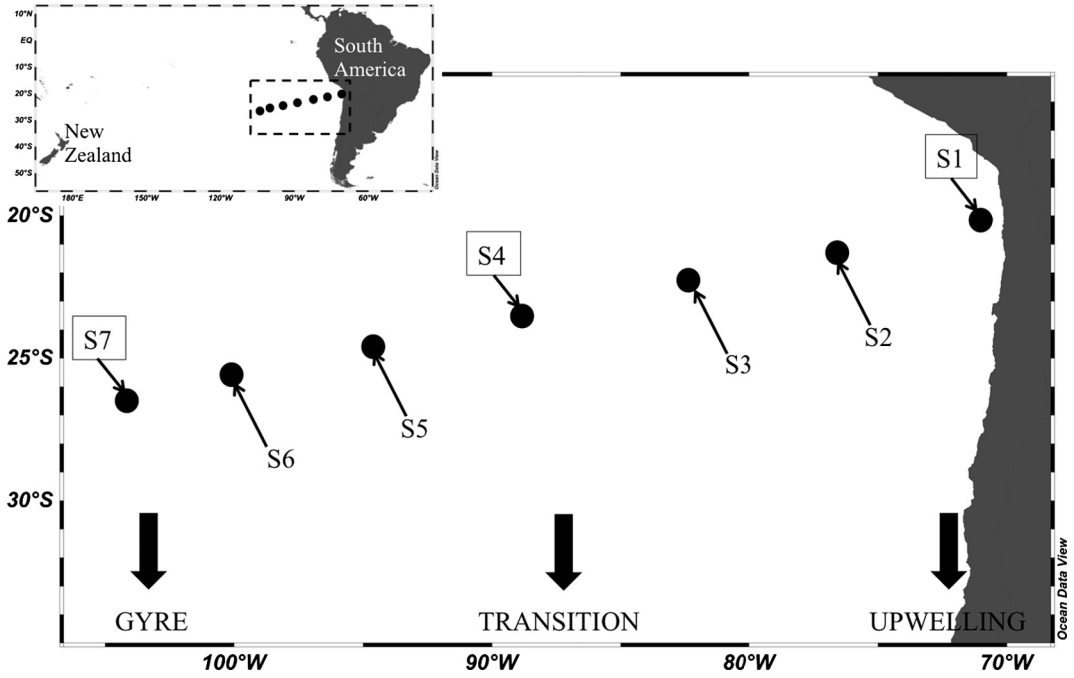

Fig. 1. Top left corner: map of the South Pacific Ocean between New Zealand and South America, with a dashed-line box locating the sampling area that is described in more detail in the map below. Station locations (S1–S7) of the BiG RAPA cruise transect in the southeast subtropical Pacific Ocean (November–December 2010), over Ocean Data View coastline. Stations 1 (near Chile) to 7 (near Easter Island) were sampled once on survey stations (S2, S3, S5, and S6; occupied for one day) and two to three times on process stations (S1: upwelling (UP), S4: transition (TR), and S7: gyre (GY); occupied for 3–4 days).

upwelling [UP], S4: transition [TR] and S7: gyre [GY]). The photosynthetically active radiation (PAR) was determined using a Biospherical (QSP- 2300, S/N 4644) sensor mounted on the rosette system containing a CTD and ancillary sensors (temperature, conductivity, pressure, oxygen and fluorescence). Seawater samples were collected at 6 different depths corresponding to 50, 25, 15, 7, 3 and 1% PAR, respectively, in 12-l Niskin bottles attached to the rosette system. When the chlorophyll maximum (CM) was deeper than 1% PAR, the CM was sampled instead (i.e., S4–S7, Table 1). Except for particulate phosphorus (PartP) samples (see below), subsamples were collected without pre-filtration into acid-cleaned (10% HCl), ultra-pure water triple-rinsed (thereafter, clean) and sample-rinsed polycarbonate bottles.

2.2. Analytical measurements

Chl was measured on 0.75- to 1-l samples collected by sequential filtration onto 2, 0.6 and 0.2 μm polycarbonate filters and kept frozen (−20 °C) until analyzed. Samples were extracted in 100% acetone for 7 d in the dark at −20 °C, then measured using a Turner model AU-10 fluorometer (Optical kit P/N 10-037R (Ex 10-050R: 340–500 nm, Em 10-051R, >665 nm) before and after acidification in order to correct for pheopigments (Strickland and Parsons, 1972).

Samples for picoplankton enumeration were fixed in a final concentration of 0.2% (w/v) paraformaldehyde, flash frozen in liquid nitrogen and stored at −80 °C. Microbial cell abundances for non-pigmented (i.e., bacteria) and pigmented cells (i.e., picophytoplankton: *Prochlorococcus*, *Synechococcus* and photosynthetic picoeukaryotes; the latter hereafter being referred to as picoalgae) were determined using a BD Influx™ flow cytometer as previously described (Duhamel et al., 2012, 2014).

Samples for dissolved inorganic phosphate (Pi) determinations were immediately analyzed on board using an auto-analyzer (Technicon AutoAnalyzer II, detection limit of 10 nmol P l^{-1}). Samples for PartP determinations were prescreened through 202-μm Nitex® mesh to remove large particles and collected into clean high-density polyethylene (HDPE) bottles rinsed three times with sample, following the Hawaii Ocean Time-Series procedure. After collection samples were vacuum filtered by serial filtration of 0.75–1-l samples onto 2, 0.6 and 0.2 μm polycarbonate filters (<0.2 bars). The filters were placed into combusted and cleaned glass tubes and kept frozen (−20 °C) until analyzed following the standard protocol by Karl et al., (1991).

2.3. Phosphorus uptake

Pi and ATP uptake rates were determined using the following tracers: ^{32}Pi (orthophosphoric acid, carrier free, MP Biomedicals #64014L, 267 TBq $mmol^{-1}$) and [γ-^{33}P]ATP (adenosine-5′-triphosphate, >90% ATP [γ-^{33}P], #35020, 111 TBq $mmol^{-1}$, hereafter G-ATP) as well as [^{3}H]ATP (adenosine-5′-triphosphate, ATP [2,8-^{3}H], #24009, 1.67 TBq $mmol^{-1}$, hereafter H-ATP), respectively. The two forms of radiolabeled ATP, G-ATP or H-ATP, were used to test if microorganisms consume ATP as a source for P and/or a source for nucleosides (adenosine), respectively. Samples were incubated for several hours in 75-ml polycarbonate bottles in on-deck, blue-shielded Plexiglas (Arkema 2069, 1/4″ thickness) incubators cooled with running surface seawater. Bottles were placed into mesh bags approximating the PAR level at which samples were taken: 50, 25, 15, 7, 3 and 1% PAR (or CM when deeper than the 1% PAR). After incubation, 10-ml seawater samples were filtered onto 2, 0.6 and 0.2 μm polycarbonate filters at low pressure (<0.6 bars). For samples incubated with G-ATP, the filtrate was collected in a separate set of tubes to determine ATP hydrolysis (see below). Filters were rinsed 3 times with 0.2 μm filtered seawater from the same sampling location. The tubes containing the filtrates to determine ATP hydrolysis were removed prior to rinsing the filters. For whole water total radioactivity, 100 μl was collected from each incubation bottle. Samples for total activity and filters were transferred into 6.5-ml HDPE scintillation vials. A 4-ml aliquot of scintillation cocktail (Ultima Gold™ LLT, Perkin Elmer) was added to the scintillation vials and samples were counted on a Beckman LS6500. The linearity of the P uptake over the incubation time was checked regularly by subsampling incubations four times over the course of an experiment and determining particulate radioactivity.

2.4. Uptake of Pi released by ATP hydrolysis

The assay was based on hydrolysis of ^{33}Pi from [γ-^{33}P]ATP and measured both release of ^{33}Pi and uptake of released ^{33}Pi as described elsewhere (Ammerman and Azam, 1985, 1991a,b; Ammerman, 1993). In brief, 9-ml of the 0.2 μm filtrate from samples used to measure ATP uptake (see above) was mixed with 1-ml of an activated charcoal slurry (20 mg charcoal ml^{-1} in 0.03 N H_2SO_4) and subsequently filtered through a 0.45-μm filter (Millipore HA). A 1-ml aliquot of this filtrate was then analyzed by scintillation counting as described above. Killed samples were prepared to assess abiotic hydrolysis of ATP, which was negligible.

Table 1
Description of the study area: station (Stn) and cast (Cast) numbers, latitude (°S) and longitude (°W), chlorophyll maximum depth (CM, m), 50% and 1% PAR depths (m). Data measured at a depth corresponding to 50% PAR: temperature (SST, °C), salinity (Sal), density anomalies (σ_0), total microbial cell abundance (Cell, $\times 10^6$ cell l^{-1}), chlorophyll *a* (Chl, μg l^{-1}), phosphate (Pi, nmol l^{-1}), particulate phosphate (PartP, nmol l^{-1}), phosphate turnover time (Pi TT, d), [γ-^{33}P] adenosine-5′-triphosphate turnover time (G-ATP TT, d) and [^{3}H] adenosine-5′-triphosphate turnover time (H-ATP TT, d).

Stn	Cast	Latitude (°S)	Longitude (°W)	Depth (m)			SST (°C)	Sal	50% PAR data							
				CM	50% PAR	1% PAR			σ_0	Cell ($\times 10^6$ cell l^{-1})	Chl (μg l^{-1})	Pi (nmol l^{-1})	PartP (nmol l^{-1})	Pi TT (d)	G-ATP TT (d)	H-ATP TT (d)
1	4	20°5.76	70°47.99	17	6	42	14.96	34.72	25.016	1660	0.336	784	58	33	3	110
1	15	20°5.00	70°47.99	24	24	n.d.	14.67	34.67	25.717	2020	0.790	1650	63	n.d.	n.d.	n.d.
2	21	21°10.64	76°34.35	50	10	65	17.94	34.95	25.249	1310	0.315	492	65	31	15	48
3	25	22°15.65	82°20.87	n.d.	12	n.d.	17.92	34.83	25.164	870	n.d.	440	34	31	n.d.	n.d.
4	29	23°27.50	88°46.08	112	14	94	18.74	35.27	25.295	621	0.098	340	29	43	25	88
4	32	23°27.50	88°46.08	110	14	n.d.	18.71	35.27	25.297	680	n.d.	330	22	60	n.d.	n.d.
4	37	23°27.50	88°46.09	120	15	95	18.62	35.24	25.302	560	0.071	344	16	76	40	59
5	44	24°33.61	94°43.48	125	15	n.d.	19.65	35.43	25.182	410	n.d.	280	16	92	n.d.	n.d.
6	50	25°33.07	100°8.13	125	17	113	20.69	35.56	25.011	350	0.035	224	11	112	24	92
7	57	26°14.92	103°57.50	180	14	94	21.53	35.80	24.956	260	0.022	210	8	151	25	55
7	61	26°14.89	103°57.64	165	15	106	21.62	35.84	24.963	266	0.023	210	9	138	21	84

2.5. Phosphorus uptake kinetic experiments

Seawater collected at a depth corresponding to 50% PAR (Table 1) was amended with 5–7 different concentrations of either Pi or ATP in order to investigate the P uptake kinetics of ^{32}Pi or G-ATP (i.e., Michaelis-Menten Kinetics). The incubation experiments received Pi amendments of 25, 150, 750, 2500 and 5000 nmol l^{-1} at UP and of 10, 25, 50, 75 and 150 nmol l^{-1} at TR and GY, with an additional amendment of 300 nmol l^{-1} at TR; or ATP amendments of 10, 20, 50, 100 and 150 nmol P-ATP l^{-1} with additional amendments of 250 and 200 nmol P-ATP l^{-1} at UP and GY, respectively. A control with no addition was also prepared. To calculate the kinetic parameters (see below), the total Pi or ATP concentration (i.e., initial + added) was taken into account.

2.6. Bioavailability factors

The relative bioavailability of different organic P compounds was determined by calculating their bioavailability factor (BF) as previously described by Björkman and co-authors (Björkman and Karl, 1994; Björkman et al., 2000). BF is estimated from the isotope dilution effect of ^{32}Pi uptake caused by the competition from selected DOP sources. Five different DOP compounds were used in separate incubations to asseses their respective BF: glucose-1-phosphate (G1P), glucose-6-phosphate (G6P), guanosine-5′-triphosphate (GTP), adenosine monophosphate (AMP) and ATP. Seawater collected at a depth corresponding to 50% PAR was amended with 300 nmol l^{-1} of either G1P, G6P, GTP, AMP or ATP. Additionally, three controls were prepared: a control using organic substrate without P was amended with 300 nmol l^{-1} glucose (Glc), a positive control was amended with 300 nmol l^{-1} phosphate (Pi) and a negative control was unamended. Samples were then incubated with ^{32}Pi as described above.

2.7. Calculation and statistical analysis

The ^{32}Pi or ATP turnover times (TT, h) and Pi uptake rates (nmol l^{-1} h^{-1}) were calculated as follows: $TT = R_T/R_F$; uptake rate = S/TT, respectively, using the radioactivity on the filter per unit incubation time (R_F, Bq l^{-1} h^{-1}), the total tracer added (R_T, Bq l^{-1}) and the Pi concentration (S, nmol l^{-1}). Uptake rates were corrected for isotope dilution induced by either the ambient or added ^{32}Pi concentration. Total ATP hydrolysis, uptake of Pi released by ATP hydrolysis and the fraction of coupled uptake of Pi released by ATP hydrolysis were calculated as follows: ATP hydrolysis (% h^{-1}) = $100 \times [(R_f + R_{fe})/R_t]/t$; uptake of Pi from ATP (% h^{-1}) = $100 \times (R_f/R_t)/t$; fraction of coupled uptake of Pi released by ATP hydrolysis = $100 \times [R_f/(R_f + R_{fe})]$, using the radioactivity on the filter, in the filtrate after charcoal extraction and the total sample (R_f, R_{fe}, R_t, respectively, dpm ml^{-1}) and t, the incubation time.

The Pi and ATP uptake kinetic parameters were calculated using Prism 6 (GraphPad Inc.). Kinetic parameters, K_m and V_{max}, were derived from non-linear regression using the Michaelis-Menten enzyme kinetics model $V = V_{max} \times S/(K_m + S)$ with V the P uptake velocity (nmol l^{-1} d^{-1}), V_{max} the maximum P uptake velocity (nmol l^{-1} d^{-1}, which shortens in response to increased substrate limitation), K_m the Michaelis-Menten constant (i.e., the substrate concentration where half-maximum uptake velocity is reached, nmol l^{-1}, reflects the relative ability of microorganisms to use low levels of substrate) and S the total substrate concentration (Pi or ATP, nmol l^{-1}). Note that V_{max} is biomass-dependent while K_m is not (e.g., Button, 1985).

The bioavailability factor (BF) was calculated as follows: BF = (TE − TN)/(TP − TN), where TE = Pi pool turnover time in the experimental treatment (tested substrate added), TN = Pi pool turnover time in the negative control (no addition) and TP = Pi pool turnover time in the positive control (Pi added). In theory, BF ranges from 0 to 1, with a value of 0 corresponding to an unavailable substrate and a value of 1 corresponding to a P compound that has a bioavailability equal to that of Pi.

Integrated values are between the surface (i.e., 0 m) and either 1% PAR depth (Stn UP) or the CM depth when 1% PAR was shallower than the CM (i.e., Stn GY and TR; Table 1). Values averaged over the euphotic layer (Z_{eu} average values) correspond to the mean of data recorded at the 6 sampled light level depths (i.e., 50, 25, 15, 7, 3 and 1% PAR). Results are reported as mean ± standard deviation (SD; number of observations: n). We used Prism 6 for the statistical analysis. Significance is reported where $p \leqslant 0.05$. Flow cytometry data were analyzed using FlowJo 7 software (Tree Star, Inc.). Section plots were drawn using Ocean Data View (ODV 4) with MATLAB default color scale, gridded field 45 per mille x and y scale-length and auto adjust color mapping.

3. Results

3.1. Description of the study area

The temperature and salinity measured at 50% PAR depth (i.e., within the mixed layer, except at S1 and S2 where the mixed layer was only a few meters deep) increased by 6.7 °C and 1.12, respectively between S1 and S7 (Fig. 1, Table 1). S1 and S2 presented the largest vertical variability in temperature, salinity, potential density and oxygen (Fig. 2). In particular, at S1, oxygen concentration decreased from ~280 μmol l^{-1} in the surface, to <2 μmol l^{-1} below 100 m, but was >55 μmol l^{-1} in the top 43 m (i.e., Z_{eu}). At S2 and S3, oxygen concentration also decreased with depth but stayed above 15 and 180 μmol l^{-1}, respectively, in the upper 200 m and was >240 μmol l^{-1} within the Z_{eu} at S2C21. The 50% PAR depth was more variable between S1 and S3 (5–12 m) than S4–S7 (15 ± 1 m, Table 1). The depths of the 1% PAR and CM increased between S1 and S7, ranging from minimum values of 42 and 17 m, respectively, at S1 to maximum values of 106 and 180 m, respectively, at S7. The CM was shallower than 1% PAR at S1 and S2 but was deeper from S3 to S7. The 1% PAR was located below the nutricline at S1, a few meters above the nutricline at S2 and was well above after S3 (Fig. 2).

3.2. Microbial abundance and biomass distributions

Total microbial cell abundances (i.e., non-pigmented bacteria plus picophytoplankton) decreased ~8-fold along the transect, ranging from 2020×10^6 cell l^{-1} at S1 to 260×10^6 cell l^{-1} at S6, at the 50% PAR depth (Table 1). Non-pigmented bacteria, *Prochlorococcus*, *Synechococcus* and picoalgae abundances were highest in the upper layer of the euphotic zone and decreased with depth within the top 100 m at S1 and S2 (Fig. 3). *Prochlorococcus* distribution at stations in or near the upwelling did not co-vary well with Chl distribution, as contributions from larger phytoplankton are expected to be more important to the Chl signal in productive waters. Yet, the maxima in *Prochlorococcus* and picoalgae cell abundances tended to be progressively deeper along the east-west transect, likely contributing to the deepening in CM observed in oligotrophic stations between S4 and S7 (Fig. 3F). The concentration of total Chl also showed strong gradients from 1.34 to 0.022 μg l^{-1} within the Z_{eu} with the minimum values at 50% PAR at S7 and maximum values between 50 and 7% PAR at S1 (Fig. 3F). Z_{eu} integrated Chl at S7 was nearly half of that at S1 (Table 2). On average more than half of the Chl at S1 (24–89%, mean = 61 ± 24%, n = 12) was in the >2 μm size fraction while this size class contributed approximately one quarter (7–31%, mean = 25 ± 9%, n = 12) at S7 (Fig. 4). In contrast the 0.2–0.6 and 0.6–2 μm fractions

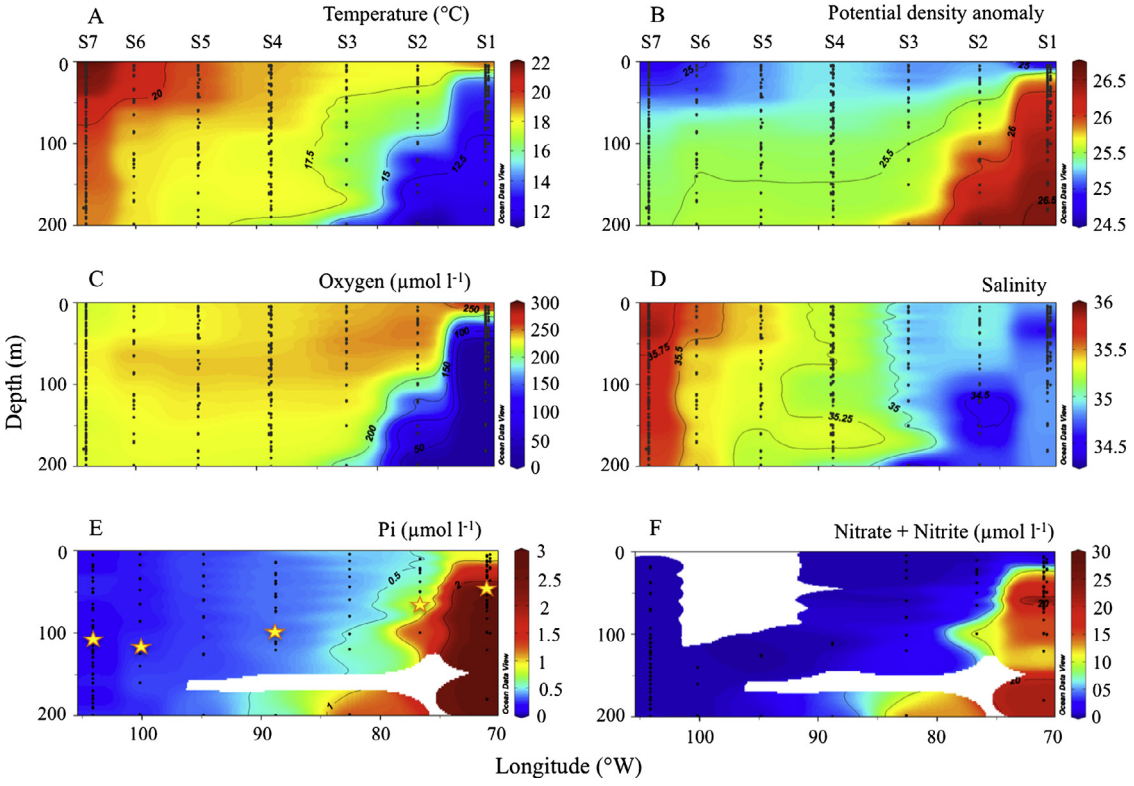

Fig. 2. Hydrological section along the BiG RAPA transect. (A) Temperature (°C), (B) potential density anomaly, (C) oxygen (µmol l^{-1}), (D) salinity (Practical Salinity Scale 1978), (E) phosphate (Pi, µmol l^{-1}) and (F) Nitrate + Nitrite (µmol l^{-1}). The black dots are for measured points. Note that the missing data on plot F compared to E are due to values below the detection method for Nitrate + Nitrite (DL = 0.1 µmol l^{-1}). The stars represent the measured 1% PAR depth.

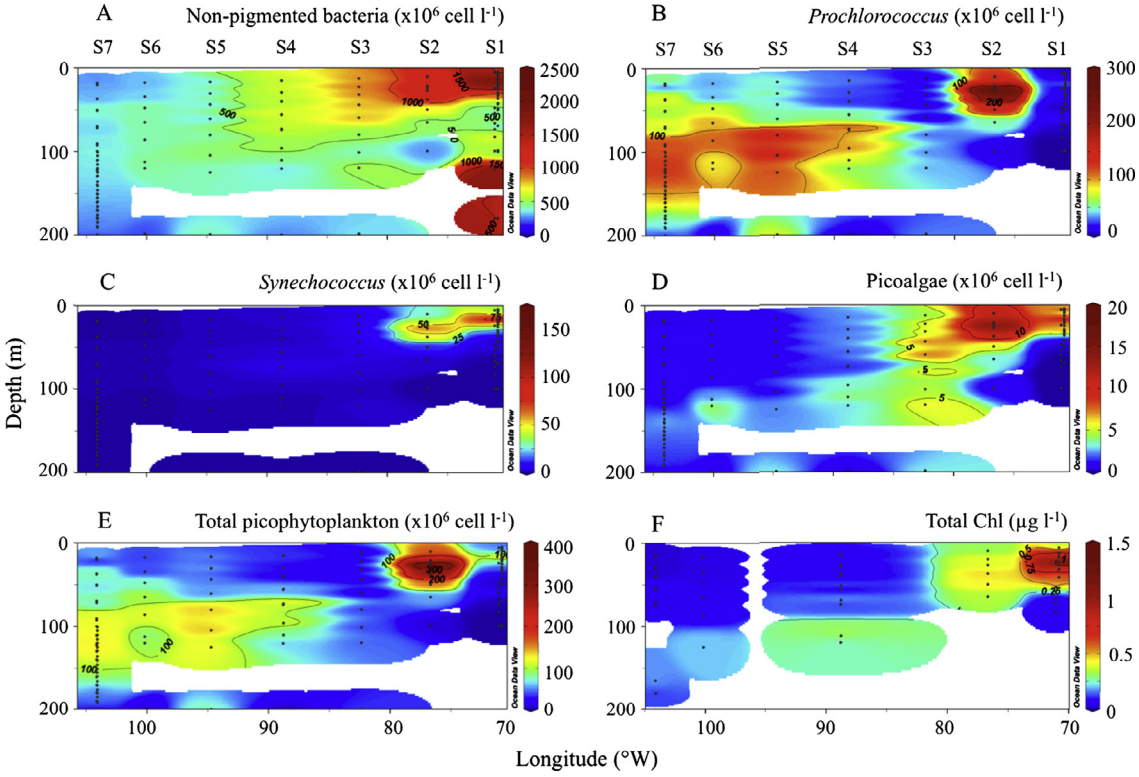

Fig. 3. Depth profiles of A: non-pigmented bacteria, B: *Prochlorococcus*, C: *Synechococcus*, D: picoalgae, and E: total picophytoplankton cell abundances (×10^6 cell l^{-1}), and F: total chlorophyll *a* concentration (total Chl, µg l^{-1}) along the longitudinal transect. The sampling locations are identified by black dots.

Table 2
Z_{eu} (m) integrated values of chlorophyll *a* (Chl, mg m^{-2}), phosphate (Pi, mmol m^{-2}), particulate phosphate (PartP, mmol m^{-2}), and phosphate uptake rate (Pi uptake, mmol m^{-2} d^{-1}), for stations (Stn) and casts (Cast).

Stn	Cast	Z_{eu} (m)	Chl (mg m^{-2})	Pi (mmol m^{-2})	PartP (mmol m^{-2})	Pi uptake (mmol m^{-2} d^{-1})
1	4	0–42	32.1	64	2.6	1.28
2	21	0–65	25.4	37	4.0	0.83
4	29	0–112	18.6	38	2.9	0.92
4	37	0–120	13.6	42	1.9	0.47
6	50	0–125	8.8	29	1.6	0.25
7	57	0–180	11.4	38	1.7	0.26
7	61	0–165	11.8	35	1.5	0.26

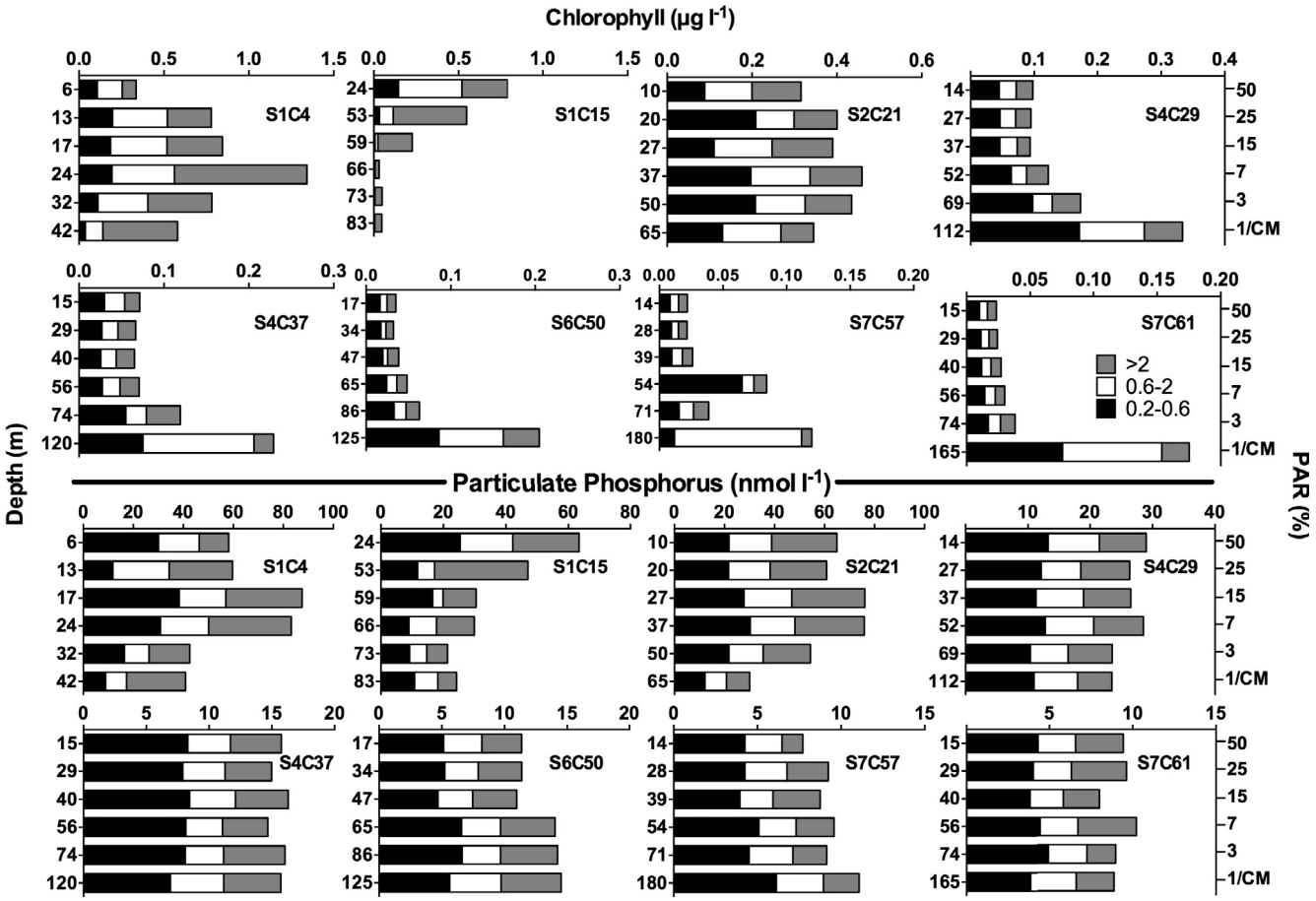

Fig. 4. Depth profiles (in meters, left y-axis; and as a fraction of PAR (%), right y-axis) of chlorophyll *a* (µg l^{-1}, top 8 plots) and particulate phosphorus (nmol l^{-1}, bottom 8 plots), for the size fractions >2 (grey bars), 0.6–2 (white bars) and 0.2–0.6 µm (black bars). Stations (S) and cast (C) numbers are given for each plot. Note that for S1–S2 and S4–S7, the bottom depths are 1% PAR and CM, respectively.

contained most of the Chl at S7 (mean = 43 ± 15% and 32 ± 18%, respectively) whereas these smaller size classes contributed 13 ± 9% and 26 ± 16% of the Chl at S1, respectively. The longitudinal distribution of total PartP also showed wide variations ranging from 7.7 to 87.5 nmol l^{-1} in the Z_{eu} with minimum values at 50% PAR at S7 and maximum values between 50 and 7% PAR at S1. Z_{eu} integrated PartP at S7 was ~1.7-fold lower than at S1 (Table 2). Similar to Chl, the >2 µm fraction contributed a larger proportion of PartP at S1 (20–64%, mean = 38 ± 12%, n = 12) but was closely followed by the 0.2–0.6 µm fraction (20–54%, mean = 37 ± 11%, n = 12), illustrating the contribution of heterotrophic bacteria and potentially detritus to PartP in the smallest size fraction. Although total PartP concentrations were lower at S7 than at S4 (*t*-test, $p < 0.05$), the relative contribution of the 3 size fractions was not significantly different between those stations (*t*-test, $p > 0.05$; 48 ± 5, 25 ± 3, 27 ± 5% for 0.2–0.6, 0.6–2, >2 µm, respectively).

3.3. Pi and ATP turnover

Pi pool turnover time ranged from 25 to 220 days (Fig. 5). Although Pi concentrations decreased from S1 to S7 (784–210 nmol l^{-1} at 50% PAR at S1C4 and S7C61, respectively, Table 1), the turnover times of Pi and G-ATP were increasingly longer (by factor of 4.2 and 7 between S1C4 and S7C61 at 50% PAR, for Pi and G-ATP, respectively) while H-ATP turnover time shortened (by a factor 1.3 between S1C4 and S7C61 at 50% PAR; Table 1 and Fig. 5). Pi turnover times were longer below 3% PAR at S1 and S2 (*t*-tests $p < 0.05$), where a sharp increase in Pi concentration was observed (Fig. 2), but there was no statistical differences at other stations (*t*-tests; Fig. 5), where Pi concentrations were more uniform within the euphotic layer. At all stations, turnover times of G-ATP were significantly more rapid than those of Pi (Z_{eu} average values of the Pi to G-ATP turnover time ratio was 14 ± 7 and

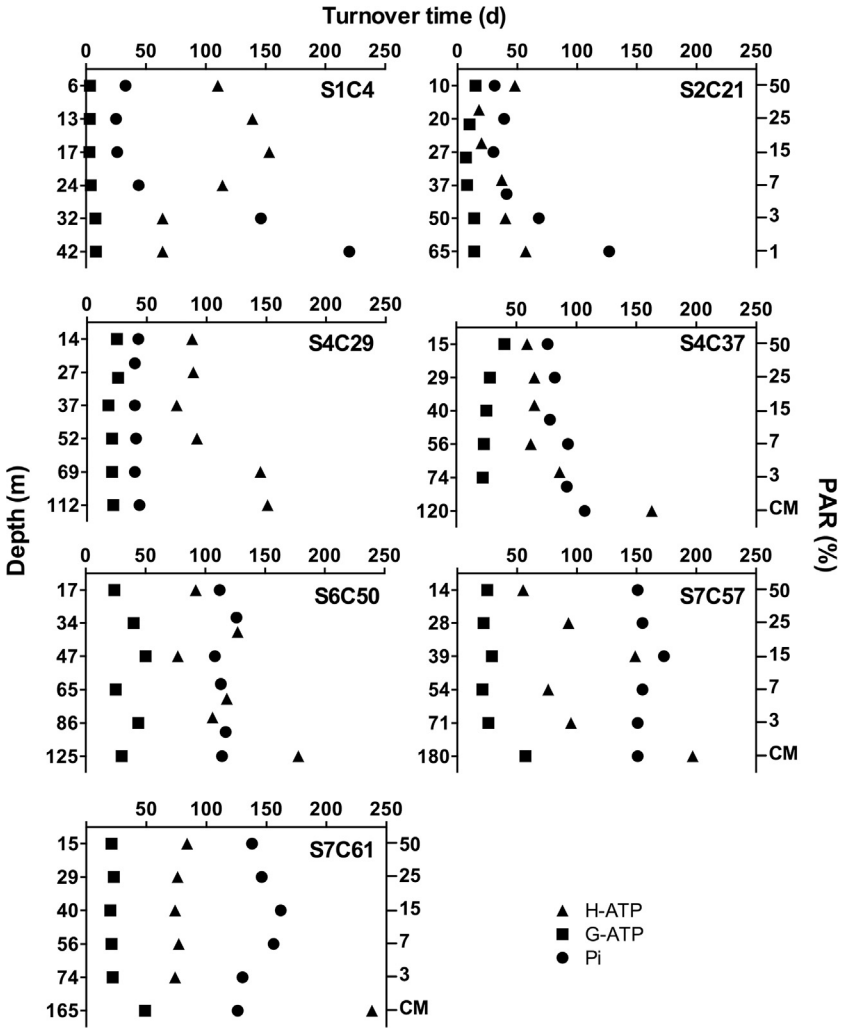

Fig. 5. Depth profiles (in meters, left y-axis; and as a fraction of PAR (%), right y-axis) of phosphate (Pi, circles), [γ-^{33}P]ATP (G-ATP, squares) and [^{3}H]ATP (H-ATP, triangles) turnover time (d). Stations (S) and cast (C) numbers are given for each plot. Note that for S4–S7 the bottom depths are CM and not 1% PAR.

6.2 ± 2.0 at S1C4 and S7C61, respectively) and H-ATP (Z_{eu} average values of the H-ATP to G-ATP turnover time ratio were 2.6 ± 0.4 and 3.8 ± 0.6 at S1C4 and S7C61, respectively) (ANOVA, $p < 0.05$, Fig. 5).

3.4. Pi and ATP uptake

Pi uptake rates ranged from 52.9 nmol l^{-1} d^{-1} at S1C4 (17 m) to 1.3 nmol l^{-1} d^{-1} at S7C57 (39 m) and were dominated by the 0.2–0.6 µm fraction (whole dataset average: 46 ± 10% of total Pi uptake, Fig. 6). PartP normalized uptake rates (the ratio of Pi uptake to PartP concentration) and cell normalized Pi uptake rates (the ratio of Pi uptake to cell abundance) also decreased from S1 to S7 (by ~3-fold at 50% PAR) and thus decreases in rates were not only driven by decreases in particle mass or cell abundance (Fig. 7). Vertical variability in Pi uptake was larger at S1 and S2 than for the other transect stations (Fig. 6), following similar trends observed for PartP (Fig. 4). The contribution of the 0.6–2 µm fraction to Pi uptake was highest at S1 and lowest at S7 (Z_{eu} average: 40 ± 9 and 21 ± 8% of total Pi uptake, respectively), but did not show a consistent trend along the transect. Interestingly, the contribution of the >2 µm fraction to Pi uptake was highest at S7C61 (Z_{eu} average: 32 ± 5% of total Pi uptake, Fig. 6, ANOVA, $p < 0.05$, *t*-tests $p < 0.05$ except for S1 which was not significantly different), similar to its contribution to PartP (Z_{eu} average: 28 ± 6% of total PartP, Fig. 4).

Total Pi uptake integrated over Z_{eu} decreased greatly from S1 to S7 (1.28 and 0.26 mmol m^{-2} d^{-1}, respectively, Table 2). There was no significant difference in the Z_{eu} average contribution of the fraction >2 µm to Pi uptake between S1 and S7 (*t*-test, $p > 0.05$, 27 ± 8%, n = 18), although there were significant variations among stations sampled along the transect (ANOVA, $p < 0.05$, Fig. 6). The average contribution of the fraction 0.2–0.6 µm to Pi uptake within the Z_{eu} significantly increased from 33 ± 7 (S1C4) to 47 ± 5% (S7C61) while the contribution of fraction 0.6–2 µm significantly decreased from 40 ± 9 (S1C4) to 21 ± 8% (S7C61). However, the contribution of the 0.6–2 µm fraction to total Pi uptake was not statistically different between stations from S4 to S7 (ANOVA, $p > 0.05$, n = 30).

The total (i.e., the sum of the three size fractions in Table 3) fraction of coupled uptake of Pi released by ATP hydrolysis was larger at S1 than S7 and was lower at 1% PAR (6.9 and 1.9%, respectively) than at 50% PAR (11.7 and 4.1%, respectively), although it did not vary widely between 50 and 3% PAR depths. The fraction of coupled uptake of Pi released by ATP hydrolysis was dominated by the 0.2–0.6 µm fraction at all stations and depths of Z_{eu} (average: 62 ± 11% of the total (>0.2 µm), n = 36, Table 3). When pooling all the data (all stations and depths of Z_{eu}), the >0.6 µm fraction was

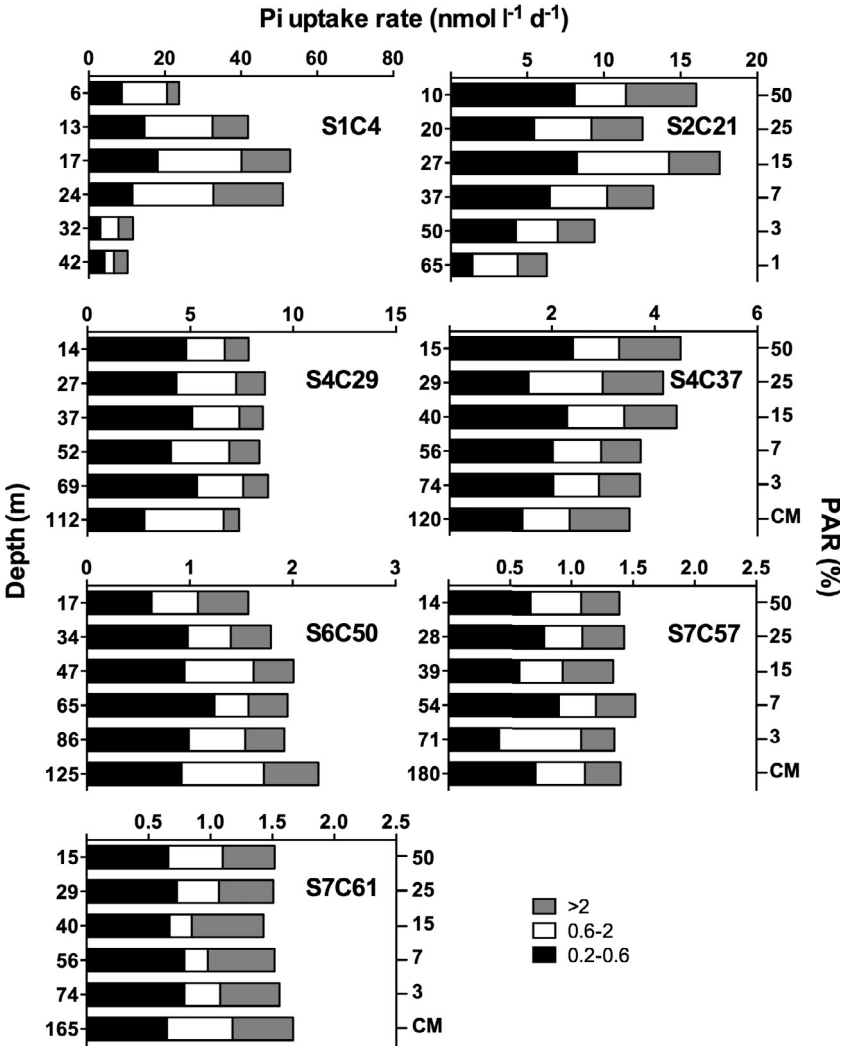

Fig. 6. Depth profiles (in meters, left y-axis; and as a fraction of PAR (%), right y-axis) of phosphate uptake rates (Pi uptake rate; nmol l^{-1} d^{-1}) for the size fractions >2 (grey bars), 0.6–2 (white bars) and 0.2–0.6 μm (black bars). Stations (S) and cast (C) numbers are given for each plot. Note that for S1–S2 and S4–S7, the bottom depths are 1% PAR and CM, respectively.

responsible for over a third (38 ± 11%, n = 36) of the coupled uptake of Pi released by ATP hydrolysis. At 50% PAR, the 0.2–0.6 μm fraction took up 2.5–6.8% of the Pi released by ATP hydrolysis over the entire transect, while the >2 μm fraction took up only 0.3–0.8%.

3.5. Kinetic response to increasing Pi or ATP

The relatively high ambient Pi concentrations and long turnover times measured along this transect suggest that Pi was potentially at biologically saturating levels relative to Pi requirements for growth. This was also illustrated in the low and variable kinetic responses to increased Pi additions, making the determination of K_m unreliable (high calculated uncertainty, Table 4). V_{max} for Pi uptake (>0.2 μm) had a smaller associated uncertainty than K_m, but could only be measured at two stations in the transition section of the transect where it was 10.84 ± 3.28 and 5.20 ± 1.52 nmol l^{-1} d^{-1}, at S4C32 and S4C37 respectively. The Pi uptake rates at ambient Pi concentrations at S4C32 and S4C37 (5.61 and 3.64 nmol l^{-1} d^{-1} at 50% PAR depth, respectively, data obtained in the control with no Pi addition used to measure the Pi uptake kinetic parameters in Table 4) were lower than V_{max} (10.84 ± 3.28 and 5.20 ± 1.52 nmol l^{-1} d^{-1}, respectively) but in the range of values within the 95% confidence interval (Table 4). For the station sampled in GY, the dataset did not fit the Michaelis-Menten model used to calculate the kinetic parameters, suggesting that ambient Pi was already saturating microbial Pi uptake.

In the case of ATP, both V_{max} and K_m gave reliable estimates as ATP turnover increased substantially with increasing additions of ATP (Table 4). V_{max} decreased from S1 to S7 (0.51 ± 0.04–0.10 ± 0.01 nmol l^{-1} d^{-1}, respectively). K_m values were 2.93 ± 0.98 and 6.28 ± 1.04 nmol l^{-1} at S1 and S7, respectively, which are all substantially higher than dissolved ATP concentrations previously reported in other marine environments (Azam and Hodson, 1977; Nawrocki and Karl, 1989; Björkman and Karl, 2005). Size fractionated data showed that at S1 the 0.2–0.6 μm fraction presented higher V_{max} than the larger size classes while the reverse was true at S4 and S7 (Table 4), even after biomass normalization. Yet the K_m for the 0.2–0.6 μm fraction was consistently lower than for the largest size fractions.

3.6. Bioavailability factors

The bioavailability of the different DOP substrates tested (G1P, AMP, GTP, G6P and ATP) varied among stations and did not show a trend along the transect as for other parameters reported here

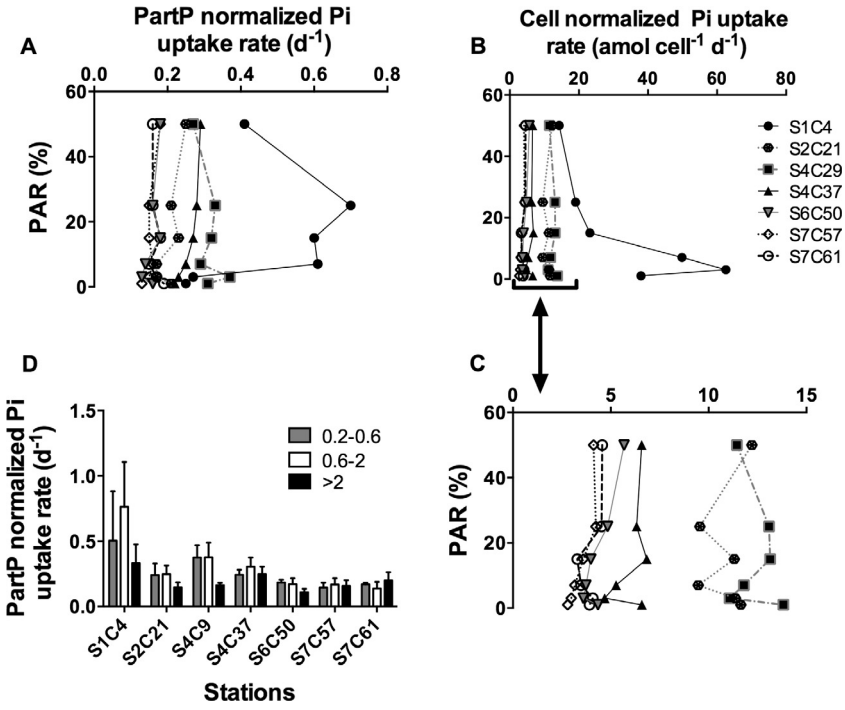

Fig. 7. Depth profiles of A: particulate phosphorus (PartP) normalized Pi uptake rate (Pi uptake rate to PartP concentration ratio, >0.2 μm fraction, d^{-1}). B and C: cell normalized Pi uptake rates (Pi uptake rate to PartP concentration ratio, >0.2 μm fraction, amol $cell^{-1}$ d^{-1}). D: Z_{eu} averaged PartP normalized uptake rate (d^{-1}) per size fraction (>2 μm: grey bars, 0.6–2 μm: white bars and 0.2–0.6 μm: black bars).

(Fig. 8). All substrates tested had their highest BF values at S1 (except for AMP at S3C25), indicating that the DOP substrate tested in this study may be more bioavailable to the microbial communities in the upwelling than at the more oligotrophic stations. BF values for DOP substrates were among the lowest at S4C43 (all <0.16).

4. Discussion

4.1. Characteristics of the BiG RAPA study area

The BiG RAPA transect showed large changes in surface salinity and temperature, Chl and cell abundance (Table 1), as would be expected when sampling from coastal to open ocean ecosystems. There were also large changes in the vertical distribution of Chl with the CM varying from a minimum of ~17 m at S1C4 to a maximum of ~180 m at S7C57, following the 25.5 isopycnal (Fig. 2) and in the 1% PAR depth, which ranged from ~42 m to ~113 m, illustrating increasing oligotrophy from east to west. Similar trends were observed along the BIOSOPE transect which also sampled southeast subtropical waters from Chile to Easter Island, although at locations south of the BiG RAPA transect (most coastal stations at 72°W, 34°S and 70°W, 20°S for BIOSOPE and BiG RAPA, respectively) and extended north-west to the Marquesas Islands (Claustre et al., 2008). The BIOSOPE project defined the central part of the gyre as starting west of 100°W, since at this location there are two eastward flowing current veins (Stramma et al., 1995) and a strong salinity gradient that separates the most oligotrophic waters from the transition zone between the SPSG and the coastal upwelling of Chile (Claustre et al., 2008). In the present study, S7 (i.e., GY) was west of 100°W and separated from S6 by a front of salinity and is thus considered to be part of the SPSG (Fig. 2). As previously observed, this area presented very low microbial abundances and Chl concentrations throughout Z_{eu} but peaked below the 1% PAR at depths down to 180 m (Figs. 3 and 4). Yet, the CM reached even greater depths (~195 m) during the BIOSOPE transect at a station west of 120°W (STB7), where the "clearest" natural waters were defined (Morel et al., 2007). While S4–S7 presented similar depth patterns of microbial and physical parameters, S1–S3 were quite variable. Indeed, variability at UP is illustrated by the differences in Chl and PartP profiles between S1C4 and S1C15 (Fig. 4). This spatial variability is likely to be driven by changes observed in the depth of the oxygen minimum relative to the 1% PAR (the oxygen minimum was below 50 m at S1C4 and S1C15 while 1% PAR depth was 42 m and 83 m, respectively).

Flow cytometric enumeration of picophytoplankton revealed that *Synechococcus* dominated at UP but greatly decreased westwards (total abundances integrated over Z_{eu} were ~50-fold greater at UP than at GY), being replaced by *Prochlorococcus* in the more oligotrophic stations with maximal abundance at the CM (Fig. 3). Picoalgal abundance followed a similar pattern of distribution to that of *Prochlorococcus* but total abundances integrated over Z_{eu} decreased ~4-fold between UP and GY while it increased ~50-fold for *Prochlorococcus*. Worden et al. (2004) showed that at a Pacific Ocean coastal site in the Southern California Bight, *Synechococcus* may be numerically dominant not only because of high growth rates but also because grazing pressure on this group is lower than on *Prochlorococcus* and picoalgae. Here we found that at the coastal site UP, the 0.6–2 μm fraction, previously showed to be dominated by *Synechococcus* (Duhamel et al., 2007), could potentially grow ~2 times faster than the smaller and larger microbes (Fig. 7D). Other factors that could explain *Synechococcus* dominance over *Prochlorococcus* in nutrient-rich coastal waters include *Synechococcus* capacity to tune its phycobilisome antenna systems to acclimate to changing temperatures and its lower susceptibility to copper toxicity than *Prochlorococcus* (for review see Biller et al., 2015). Applying the carbon conversion factors determined by Grob et al. (2007) during the BIOSOPE transect (29, 60, 730 fg C $cell^{-1}$ for *Prochlorococcus*, *Synechococcus* and picoalgae, respectively), we found that *Prochlorococcus*, *Synechococcus* and

Table 3
Total ATP hydrolysis (% h^{-1}), uptake of Pi released by ATP hydrolysis (% h^{-1}), and fraction of coupled uptake of Pi released by ATP hydrolysis (%) per stations (Stn), casts (Cast) and sampling depth (as % PAR). Values are reported for various size fractions.

Stn	Cast	% PAR	Total ATP hydrolysis	Uptake of Pi released by ATP hydrolysis (% h^{-1})			Fraction of coupled uptake of Pi released by ATP hydrolysis (%)		
			(% h^{-1})	0.2–0.6	0.6–2	>2 μm	0.2–0.6	0.6–2	>2 μm
1	4	50	10.86	0.74	0.47	0.06	6.83	4.33	0.53
		25	12.07	0.90	0.40	0.04	7.43	3.33	0.35
		15	11.24	0.99	0.37	0.06	8.83	3.28	0.54
		7	10.95	0.74	0.21	0.08	6.74	1.93	0.77
		3	7.93	0.37	0.13	0.04	4.68	1.60	0.44
		1	7.25	0.24	0.21	0.05	3.31	2.86	0.73
4	29	50	4.36	0.12	0.03	0.01	2.71	0.77	0.32
		25	3.93	0.12	0.03	0.01	3.01	0.79	0.35
		15	4.66	0.17	0.05	0.01	3.70	0.97	0.30
		7	4.18	0.11	0.07	0.02	2.67	1.67	0.48
		3	3.90	0.12	0.07	0.01	3.02	1.72	0.32
		1	3.57	0.18	0.06	0.02	4.99	1.64	0.47
4	37	50	2.48	0.08	0.02	0.01	3.04	0.76	0.37
		25	2.56	0.12	0.02	0.01	4.66	0.83	0.29
		15	2.60	0.13	0.03	0.01	5.09	1.05	0.36
		7	2.66	0.14	0.04	0.01	5.12	1.42	0.34
		3	2.66	0.14	0.04	0.01	5.37	1.32	0.36
		1	1.91	0.00	0.00	0.00	0.05	0.04	0.06
6	50	50	2.78	0.11	0.05	0.02	3.93	1.85	0.55
		25	2.41	0.07	0.03	0.01	2.82	1.09	0.40
		15	2.34	0.03	0.03	0.02	1.36	1.38	0.80
		7	2.71	0.10	0.05	0.02	3.78	1.92	0.56
		3	2.43	0.03	0.05	0.01	1.38	1.94	0.58
		1	2.41	0.08	0.04	0.02	3.47	1.63	0.72
7	57	50	2.57	0.10	0.04	0.02	4.06	1.63	0.77
		25	2.54	0.12	0.04	0.02	4.90	1.67	0.80
		15	2.42	0.08	0.04	0.02	3.51	1.66	0.76
		7	2.88	0.12	0.06	0.02	4.14	2.23	0.61
		3	2.75	0.09	0.05	0.02	3.45	1.78	0.57
		1	2.32	0.05	0.02	0.00	2.27	0.72	0.18
7	61	50	4.82	0.12	0.05	0.03	2.50	1.08	0.53
		25	4.84	0.10	0.06	0.02	2.09	1.22	0.38
		15	4.75	0.12	0.07	0.02	2.43	1.51	0.50
		7	4.81	0.11	0.07	0.02	2.18	1.52	0.47
		3	4.81	0.11	0.06	0.02	2.29	1.26	0.41
		1	4.41	0.06	0.02	0.01	1.26	0.53	0.12

picoalgae represented on average 1, 37 and 62%, respectively, of the total integrated picophytoplankton carbon biomass at UP and 79, 1 and 20%, respectively, at GY. In a separate study from the BiG RAPA cruise, Rii et al. (2016) showed that picoalgae contributed to 36–48% of euphotic zone depth-integrated picophytoplankton primary productivity (^{14}C-primary productivity derived from flow cytometric sorting of radiolabeled cells). The large contribution of picoalgae to primary production and picophytoplankton carbon biomass suggests that they potentially also make a large contribution to P uptake rates and export along the transect. As was observed for picophytoplankton, non-pigmented bacteria abundance decreased substantially from UP to GY, but they still dominated total picoplankton abundance (96 ± 3% and 79 ± 5%, respectively). Hence, bacteria may have an important role in P cycling as indicated by the dominant contribution of the 0.2–0.6 μm fraction to total Pi uptake rate (Fig. 6 and Table 4).

4.2. P stocks, turnover time and DOP bioavailability

As for microbial abundance and Chl concentration, PartP decreased from east to west and was about 6 times lower at GY than at UP. Although Pi also greatly decreased, it remained relatively high along the BiG RAPA transect, even in the oligotrophic GY (Pi > 210 nmol l^{-1}) as previously observed by Moutin et al. (2008). As a consequence, the turnover times of Pi remained relatively long (>248 d), suggesting that microorganisms were Pi-replete or the demand for P was low. Results from kinetic parameters for Pi uptake indeed showed that Pi was at saturating concentration at GY (Table 4) and cell normalized Pi uptake rates were significantly lower at GY than at UP (*t*-tests $p < 0.05$, Fig. 7). Yet, ATP was utilized by microorganisms both for the Pi and for adenosine, and the estimated turnover times were shorter than for Pi (G-ATP > 3 d, H-ATP > 48 d, Table 1). These findings suggest that while Pi turnover is strongly affected by Pi concentrations, there is no effect on G-ATP turnover, supporting the claim that ATP processing is independent of Pi concentration (Ammerman and Azam, 1985, 1991a; Björkman et al., 2012). These results also support previous findings based on alkaline phosphatase activity as a proxy for DOP utilization, which suggested that microorganisms use DOP for their P nutrition even in the Pi-replete SPSG (Duhamel et al., 2011). In the present study, the total ATP hydrolysis rates varied between 10.86 and 1.91% h^{-1} (average 4.4 ± 2.8% h^{-1}) along the entire transect and upper water column, suggesting that the ambient dissolved ATP pool turned over relatively rapidly (9–52 h, 29 ± 12 h) in comparison to the particulate fraction, indicating that dissolved ATP is a bioavailable pool of P in the southeast subtropical Pacific Ocean.

The relative utilization of DOP compared to Pi is likely to depend on the composition and energy density of the DOP and, possibly, the redox state of P. In order to evaluate the bioavailability of a range of DOP compounds compared to that of Pi, we performed bioassays as described in Björkman and Karl (1994). DOP

Table 4
Kinetic (V_{max}, nmol l^{-1} d^{-1}; and K_m, nmol l^{-1}) parameters for ATP and Pi uptake. The best-fit values are given along with the 95% confidence intervals. Parameters verifying the goodness of fit (n = number of data, r = correlation coefficient) are also given. No-fit (NF) means that the dataset did not fit the Michaelis-Menten model used to calculate the kinetic parameters.

	Station	Fraction	Best-fit values		95% confidence intervals		Goodness of fit	
			V_{max}	K_m	V_{max}	K_m	n	r
ATP	S1C15	>0.2	0.51 ± 0.04	2.93 ± 0.98	0.38–0.63	0.0–6.0	5	0.98
		0.2–0.6	0.30 ± 0.03	1.55 ± 0.79	0.22–0.38	0.0–4.1	5	0.94
		0.6–2	0.16 ± 0.02	10.24 ± 3.42	0.12–0.21	0.7–19.7	6	0.95
		>2	0.12 ± 0.02	17.13 ± 8.44	0.06–0.17	0.0–40.6	6	0.93
	S4C32	>0.2	0.35 ± 0.03	30.15 ± 6.64	0.26–0.43	13.1–47.2	7	0.99
		0.2–0.6	0.11 ± 0.03	18.34 ± 11.11	0.03–0.19	0.0–737	6	0.94
		0.6–2	0.38 ± 0.39	165 ± 222	0.0–1.40	0.0–737	7	0.96
		>2	1.22 ± 2.79	761 ± 1866	0.0–8.40	0.0–5559	7	0.99
	S4C37	>0.2	0.13 ± 0.02	7.21 ± 4.09	0.07–0.19	0.0–18.6	6	0.93
		0.2–0.6	0.04 ± 0.01	0.63 ± 1.04	0.02–0.06	0.0–3.5	6	0.70
		0.6–2	0.05 ± 0.01	7.23 ± 3.45	0.03–0.07	0.0–16.8	6	0.96
		>2	0.03 ± 0.01	28.96 ± 22.22	0.0–0.07	0.0–90.6	6	0.95
	S7C68	>0.2	0.10 ± 0.00	6.28 ± 1.04	0.09–0.12	3.4–9.2	6	0.99
		0.2–0.6	0.02 ± 0.005	1.18 ± 2.03	0.01–0.04	0.0–6.8	6	0.77
		0.6–2	0.04 ± 0.01	4.39 ± 3.97	0.02–0.07	0.0–15.4	6	0.88
		>2	0.04 ± 0.01	11.10 ± 5.79	0.02–0.06	0.0–27.2	6	0.96
Pi	S4C32	>0.2	10.84 ± 3.28	239 ± 200	2.42–19.27	0.0–752.7	7	0.62
		0.2–0.6	NF	NF	NF	NF	NF	NF
		0.6–2	6.21 ± 1.14	631 ± 196	3.28–9.13	127–1136	7	0.96
		>2	3.62 ± 1.75	1174 ± 784	0.0–8.12	0.0–3190	7	0.91
	S4C37	>0.2	5.20 ± 1.52	169.5 ± 164	0.98–9.43	0.0–626	6	0.57
		0.2–0.6	6.72 ± 7.01	1085 ± 1550	0.0–26.2	0.0–5389	6	0.77
		0.6–2	NF	NF	NF	NF	NF	NF
		>2	NF	NF	NF	NF	NF	NF
	S7C68	All	NF	NF	NF	NF	NF	NF

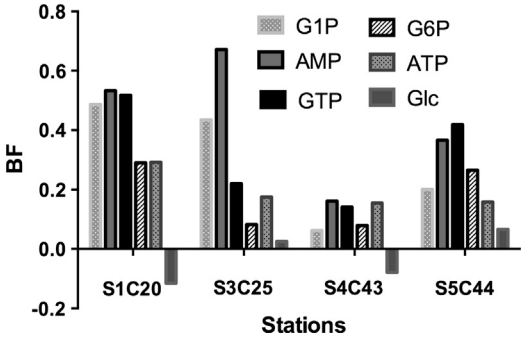

Fig. 8. Bioavailability of selected substrates to natural assemblages of microorganisms at several stations sampled in the subtropical south Pacific. Samples were amended with exogenous compounds: G1P = glucose-1-phosphate, AMP = adenosine-1-monophosphate, GTP = guanosine-5′-triphosphate, G6P = glucose-6-phosphate, ATP = adenosine-5′-triphosphate, Glc = glucose. Bioavailability factor (BF) is measured by the isotope dilution of ^{33}Pi uptake relative to a positive control sample with an equivalent inorganic phosphorus (Pi) addition, the assumed preferred substrate, and a negative control with no exogenous substrate. BF ranges from 0 (i.e., unavailable substrate) to 1 (substrate availability equivalent to that of Pi, see method for further details). Negative BF values result from a slight enhancement in Pi uptake rates in incubations with exogenous substrates relative to the negative controls.

concentrations measured in near surface waters in an area proximate to the present study (BIOSOPE cruise) varied from 440 to 175 nmol l^{-1}, in the upwelling and in the center of the gyre, respectively (Moutin et al., 2008). Considering that BF are calculated in reference to a Pi amended control and the relatively high concentrations of tested DOP substrate added, results should not be affected by ambient DOP concentration (for details, see method section). Using this approach, Björkman and co-authors found that nucleotides were the most readily utilizable of the DOP compounds tested in their studies in Hawaiian coastal waters and in the North Pacific Subtropical Gyre (Björkman and Karl, 1994; Björkman et al., 2000). Here, AMP, GTP and ATP presented BF values generally higher than glucose-phosphate substrates G1P and G6P. Yet, the BF for the same DOP compounds varied among stations, indicating that variations in the community composition may influence the bioavailability of DOP compounds to natural microbial communities. This result is in accordance with previous findings interrogating the availability of dissolved organic matter to different microbial assemblages (Judd et al., 2006; Jurgensone and Aigars, 2012). However, compositional differences in DOP cannot be completely ruled out along the transect, and the impact of that factor is unknown, but is probably of lesser importance than community composition.

4.3. Role of microbes in the southeast Pacific P cycling

Size fractionated PartP showed that the 0.2–0.6 μm fraction represented a larger contribution to total PartP in the GY than at UP (Z_{eu} average: 48 ± 5% and 37 ± 11%, respectively), illustrating the increasing importance of smaller sized organisms to biomass in oligotrophic environments. Although total PartP concentration and Pi uptake rates greatly decreased from east to west (by a maximum of ~8 and ~17-fold, respectively, at 50% PAR), the relative contribution of the three size fractions did not change significantly between S4 and S7, revealing that the role of the smaller-sized microbes was similar between TR and GY. The organisms were found to realize their maximal Pi uptake rates at or near ambient Pi concentrations, implying that Pi supply was not limiting community production and could support the microbes' requirements from UP to GY. As microorganisms were not Pi limited, particulate Pi normalized uptake rates can be used as a proxy for specific growth rates (μ, Duhamel et al., 2007) and can only provide a lower constraint on μ. As any proxy for specific growth rate, this approach presents potential biases (in particular the fraction of

detrital matter is unknown) and should be interpreted with caution. Yet, compared to using carbon-based proxies, this approach does not rely on conversion factors (e.g., carbon to Chl ratio) and provides an evaluation of specific growth rate for both autotrophic and heterotrophic organisms. As expected, Pi normalized uptake rates were higher at UP than in the rest of the transect and decreased from east to west, implying that microbial cell growth was higher in the most productive part of the transect (UP) and decreased with increasing oligotrophy (UP > TR > GY). As previously found in the southeast subtropical Pacific, the >2 μm fraction showed lower particulate Pi normalized uptake rates than the smaller fractions, suggesting that picoplankton-sized cells (0.2–2 μm) grew faster than the larger cells over a wide range of trophic conditions (Duhamel et al., 2007). Yet, at some depths at S7, the >2 μm size class showed Pi normalized uptake rates close to or even higher than those for the smaller fractions, suggesting that less abundant but larger cells were important contributors to productivity at GY.

We also investigated the potential role of DOP as a source of P for microbial nutrition along the BiG RAPA transect. To date, there are no studies reporting uptake rates and kinetic parameters for DOP utilization by microbes in this part of the world's oceans. ATP is often used as a model substrate to estimate microbial DOP utilization for its convenience as a commercially available DOP compound (Ammerman and Azam, 1985; Bentzen & Taylor, 1991; Lomas et al., 2010; Orchard et al., 2010; Björkman et al., 2012; Duhamel et al., 2012). However, as any model substrate, it may not be representative of all DOP compounds that are utilized by the microbial communities and interpretations are limited to the smaller range of DOP compound sizes and to relatively bioavailable substrates (Fig. 8). ATP, like the majority of DOP compounds, is considered to be hydrolyzed outside the cell before uptake of the Pi or other moieties, as most bacteria do not take up intact ATP (Bengis-Garber and Kushner, 1982; Ammerman and Azam, 1985). Ammerman and Azam (1991a) showed that ATP uptake is distinguishable from alkaline phosphatase activity by its substrate specificity to 5′-nucleotides and by its lack of inhibition by Pi. Yet, the coupled uptake of Pi released into the ambient water by ATP hydrolysis was inhibited due to isotope dilution (Ammerman and Azam, 1991a). Here we also found no effect of Pi addition on ATP turnover. The uptake rate of G-ATP did not saturate at ambient ATP concentration and increased significantly with the addition of ATP, suggesting that microorganisms had the potential to take up larger quantities of Pi from ATP if it was present in higher concentrations. Yet, the V_{max} and K_m of G-ATP were much lower than for Pi (Table 4), indicating that microorganisms are adapted to low ATP concentration, which they turned over more rapidly than Pi (Fig. 5). The V_{max} of G-ATP at 50% PAR decreased by ~5-fold between S1 and S7 (Table 4) and remained low in comparison to Pi uptake rates at ambient concentration (46.5 and 15.2 times lower at UP and GY, respectively, Fig. 6), suggesting that Pi uptake from ATP was a small fraction of total P uptake at ambient concentration. Yet, the K_m values for G-ATP uptake were much lower than those estimated for Pi uptake, suggesting that microbes had higher affinity for ATP than for Pi at both stations. Consequently, the contribution of P uptake from ATP relative to Pi uptake is expected to be higher in low Pi environments than in high Pi environments. In the low-Pi Sargasso Sea, Lomas et al., (2010) found that ATP uptake was lower than Pi uptake, but with a larger contribution of ATP uptake in the fall than in the spring, when Pi concentrations are the lowest. Ammerman and Azam (1991a) showed that the percent of Pi released by ATP hydrolysis decreases with increasing Pi concentration and proposed that the coupled Pi uptake is controlled by ambient Pi concentrations. Yet in the present study, the fraction of coupled uptake of Pi released by ATP hydrolysis was higher at UP, where Pi concentrations and biomass normalized Pi uptake rates were higher than at other stations. Nevertheless, turnover times of Pi and G-ATP were shorter at UP than elsewhere, suggesting that total P availability rather than Pi concentration alone may control the coupled Pi uptake. In a separate study, Ammerman and Azam (1991b) concluded that the distribution of ATP hydrolysis is determined by microbial biomass and growth rather than by Pi depletion. Thus the highest ATP hydrolysis measured at UP may also be the result of higher biomass and growth rates. The fact that <15% of the Pi released by ATP hydrolysis was assimilated by microbes suggests that the bioavailability of the ambient Pi pool was not limiting production. As previously shown for coastal environments, the majority of the uptake of Pi released by ATP hydrolysis was by the smallest fraction (0.2–0.6 μm) dominated by heterotrophic bacteria, indicating that they are the main contributor to 5′-nucleotidase activity (Ammerman and Azam, 1985, 1991a). Nonetheless, about a third of this activity was by organisms larger than 0.6 μm, implying that picophytoplankton also contribute to the cycling of nucleotides, a result in accordance with picocyanobacteria genomic data reporting genes encoding proteins with potential 5′-nucleotidase activity (Moore et al., 2005; Scanlan et al., 2009; Kathuria and Martiny, 2011). While we cannot exclude the possibility that picophytoplankton took up the Pi hydrolyzed by bacteria, the uptake of a fraction of Pi regenerated from ATP in environments with relatively large pools of ambient Pi, suggests that the uptake of Pi released by ATP hydrolysis must be physically coupled to hydrolysis. We also compared microbial use of ATP from G-ATP and H-ATP in parallel incubations, in order to test if microorganisms consume ATP as a source of P or adenosine, respectively. Results showed that the turnover time of the pool of G-ATP was significantly faster than for H-ATP (Table 1), indicating that Pi from the γ position in ATP may be preferred over adenosine. Our results also indicate that the different sample size fractions contributed to similar proportions of the total G-ATP and H-ATP uptake, suggesting that the same microbes can use ATP for both Pi and adenosine.

4.4. Conclusions

Understanding the biogeochemical cycling of nutrients is essential for interpreting the present and for predicting future effects of natural and anthropogenically induced changes in nutrient composition on marine ecosystems. The southeast subtropical Pacific presents strong gradients in all parameters measured in the present study. Three main zones could be distinguished: UP was the most productive area but also the most variable, most likely due to variations in the oxygen minimum depth; GY was the least productive due to low biomass and low particulate Pi normalized uptake rate and showed deep transmitted light penetration; TR presented intermediary conditions but as for GY, conditions were relatively uniform between stations.

Pi concentrations and turnover time remained high and Pi uptake rates were low. Even though the ambient Pi was well above limiting concentrations and cells were P-replete, microorganisms hydrolyzed and assimilated Pi from ATP, indicating that DOP could be a source of P (and perhaps of other elements) for microbial growth, or potentially for P storage as polyphosphates, independently of their P-status. Nucleotides were the most bioavailable of the DOP substrates tested here. However, <15% of the Pi hydrolyzed from ATP was assimilated by microbes, suggesting that 5′-nucleotidase activity could potentially release important quantities of Pi into the surrounding water, which may have a great impact on the role that microbes, particularly bacteria, play in ocean production and export.

The southeast subtropical Pacific presents a wide range of environmental conditions, where microbial DOP hydrolytic processes are maintained and contribute to P-cycling despite Pi-sufficiency.

Acknowledgments

We thank the Captain and crew of the R/V *Melville* for accommodating our needs. We thank Tara Clemente and Ken Doggett for their help with sampling and processing particulate phosphorus and chlorophyll samples and J. C. Jennings, Jr. for phosphate determinations. Funds for this work were provided by the Gordon and Betty Moore Foundation's Marine Microbiology Initiative (D.M. K., 3794) and the Center for Microbial Oceanography: Research and Education (C-MORE, National Science Foundation, D.M.K., EF0424599).

References

Ammerman, J.W., 1993. Microbial cycling of inorganic and organic phosphorus in the water column. In: Kemp, P.F., Sherr, B.F., Sherr, E.B., Cole, J.J. (Eds.), Handbook of Methods in Aquatic Microbial Ecology. Lewis Press, pp. 621–631.

Ammerman, J.W., Azam, F., 1985. Bacterial 5-nucleotidase in aquatic ecosystems: a novel mechanism of phosphorus regeneration. Science 227, 1338–1340. http://dx.doi.org/10.1126/science.1227.4692.1338.

Ammerman, J.W., Azam, F., 1991a. Bacterial 5′-nucleotidase activity in estuarine and coastal marine waters: characterization of enzyme activity. Limnol. Oceanogr. 36, 1427–1436.

Ammerman, J.W., Azam, F., 1991b. Bacterial 5′-nucleotidase activity in estuarine and coastal marine waters: role in phosphorus regeneration. Limnol. Oceanogr. 36, 1437–1447.

Azam, F., Hodson, R.E., 1977. Dissolved ATP in the sea and its utilisation by marine bacteria. Nature 267, 696–698.

Bengis-Garber, C., Kushner, D.J., 1982. Role of membrane-bound 5′-nucleotidase in nucleotide uptake by the moderate halophile *Vibrio costicola*. J. Bacteriol. 149, 808–815.

Bentzen, E., Taylor, W.D., 1991. Estimating organic P utilization by freshwater plankton using [^{33}P]ATP. J. Plankton Res. 13, 1223–1238.

Biller, S.J., Berube, P.M., Lindell, D., Chisholm, S.W., 2015. *Prochlorococcus*: the structure and function of collective diversity. Nat. Rev. Microbiol. 13, 13–27.

Björkman, K., Karl, D.M., 1994. Bioavailability of inorganic and organic phosphorus compounds to natural assemblages of microorganisms in Hawaiian coastal waters. Mar. Ecol. Prog. Ser. 111, 265–273.

Björkman, K.M., Duhamel, S., Karl, D.M., 2012. Microbial group specific uptake kinetics of inorganic phosphate and adenosine-5′-triphosphate (ATP) in the North Pacific Subtropical Gyre. Front. Microbiol. 3, 1–17.

Björkman, K.M., Karl, D.M., 2003. Bioavailability of dissolved organic phosphorus in the euphotic zone at Station ALOHA, North Pacific Subtropical Gyre. Limnol. Oceanogr. 48, 1049–1057. http://dx.doi.org/10.4319/lo.2003.48.3.1049.

Björkman, K.M., Karl, D.M., 2005. Presence of dissolved nucleotides in the North Pacific Subtropical Gyre and their role in cycling of dissolved organic phosphorus. Aquat. Microb. Ecol. 39, 193–203. http://dx.doi.org/10.3354/ame039193.

Björkman, K.M., Thomson-Bulldis, A.L., Karl, D.M., 2000. Phosphorus dynamics in the North Pacific subtropical gyre. Aquat. Microb. Ecol. 22, 185–198. http://dx.doi.org/10.3354/ame022185.

Bonnet, S., Guieu, C., Bruyant, F., Pril, O., Van Wambeke, F., Raimbault, P., Moutin, T., Grob, C., Gorbunov, M.Y., Zehr, J.P., Masquelier, S.M., Garczarek, L., Claustre, H., 2008. Nutrient limitation of primary productivity in the Southeast Pacific (BIOSOPE cruise). Biogeosciences 5, 215–225.

Button, D.K., 1985. Kinetics of nutrient-limited transport and microbial-growth. Microbiol. Rev. 49, 270–297.

Clark, L.L., Ingall, E.D., Benner, R., 1998. Marine phosphorus is selectively remineralized. Nature 393, 426.

Clark, L.L., Ingall, E.D., Benner, R., 1999. Marine organic phosphorus cycling: novel insights from nuclear magnetic resonance. Am. J. Sci. 2999, 724–737.

Claustre, H., Maritorena, S., 2003. The many shades of ocean blue. Science 302, 1514–1515. http://dx.doi.org/10.1126/science.1092704.

Claustre, H., Sciandra, A., Vaulot, D., 2008. Introduction to the special section bio-optical and biogeochemical conditions in the South East Pacific in late 2004: the BIOSOPE program. Biogeosciences 5, 679–691. http://dx.doi.org/10.5194/bg-5-679-2008.

Duhamel, S., Björkman, K.M., Doggett, J.K., Karl, D.M., 2014. Microbial response to enhanced phosphorus cycling in the North Pacific Subtropical Gyre. Mar. Ecol. Prog. Ser. 504, 43–58.

Duhamel, S., Björkman, K.M., Karl, D.M., 2012. Light dependence of phosphorus uptake by microorganisms in the North and South Pacific subtropical gyres. Aquat. Microb. Ecol. 67, 225–238.

Duhamel, S., Björkman, K.M., Van Wambeke, F., Moutin, T., Karl, D.M., 2011. Characterization of alkaline phosphatase activity in the North and South Pacific Subtropical Gyres: implications for phosphorus cycling. Limnol. Oceanogr. 56, 1244–1254.

Duhamel, S., Moutin, T., 2009. Carbon and phosphate incorporation rates of microbial assemblages in contrasting environments in the Southeast Pacific. Mar. Ecol. Prog. Ser. 375, 53–64. http://dx.doi.org/10.3354/meps07765MEPS.

Duhamel, S., Moutin, T., Van Wambeke, F., Van Mooy, B., Rimmelin, P., Raimbault, P., Claustre, H., 2007. Growth and specific P-uptake rates of bacterial and phytoplanktonic communities in the Southeast Pacific (BIOSOPE cruise). Biogeosciences 4, 941–956.

Dyhrman, S., Ammerman, J.W., Van Mooy, B., 2007. Microbes and the marine phosphorus cycle. Oceanography 20, 110–116.

Grob, C., Ulloa, O., Claustre, H., Huot, Y., Alarcón, G., Marie, D., 2007. Contribution of picoplankton to the total particulate organic carbon concentration in the eastern South Pacific. Biogeosciences 4, 837–852.

Judd, K.E., Crump, B.C., Kling, G.W., 2006. Variation in dissolved organic matter controls bacterial production and community composition. Ecology 87, 2068–2079.

Jurgensone, I., Aigars, J., 2012. Bioavailability of riverine dissolved organic matter to phytoplankton in the marine coastal waters. Estuar. Coast. Shelf Sci. 107, 97–104.

Karl, D.M., 2000. Phosphorus, the staff of life. Nature 406, 31–32. http://dx.doi.org/10.1038/35017683.

Karl, D.M., 2014. Microbially mediated transformations of phosphorus in the sea: new views of an old cycle. Annu. Rev. Mar. Sci. 6 (6), 279–337.

Karl, D.M., Björkman, K., 2015. Dynamics of dissolved organic phosphorus. In: Hansell, D.A., Carlson, C.A. (Eds.), Biogeochemistry of Marine Dissolved Organic Matter. second ed. Academic Press, Burlington, pp. 233–334.

Karl, D.M., Björkman, K.M., Dore, J.E., Fujieki, L., Hebel, D.V., Houlihan, T., Letelier, R. M., Tupas, L.M., 2001. Ecological nitrogen-to-phosphorus stoichiometry at station ALOHA. Deep-Sea Res. II 48, 1529–1566. http://dx.doi.org/10.1016/S0967-0645(00)00152-1.

Karl, D.M., Dore, J.E., Hebel, D.V., Winn, C., 1991. Procedures for particulate carbon, nitrogen, phosphorus and total mass analyses used in the US-JGOFS Hawaii Ocean Time-Series Program. In: Spencer, D., Hurd, D. (Eds.), Marine Particles: Analysis and Characterization. American Geophysical Union, Geophysical Monograph 63, pp. 71–77.

Kathuria, S., Martiny, A.C., 2011. Prevalence of a calcium-based alkaline phosphatase associated with the marine cyanobacterium *Prochlorococcus* and other ocean bacteria. Environ. Microbiol. 13, 74–83.

Kolowith, L.C., Ingall, E.D., Benner, R., 2001. Composition and cycling of marine organic phosphorus. Limnol. Oceanogr. 46, 309–320.

Krom, M.D., Kress, N., Brenner, S., Gordon, L.I., 1991. Phosphorus limitation of primary productivity in the eastern Mediterranean Sea. Limnol. Oceanogr. 36, 424–432.

Lomas, M.W., Burke, A.L., Lomas, D.A., Bell, D.W., Shen, C., Dyhrman, S.T., Ammerman, J.W., 2010. Sargasso Sea phosphorus biogeochemistry: an important role for dissolved organic phosphorus (DOP). Biogeosciences 7, 695–710.

Mather, R.L., Reynolds, S.E., Wolff, G.A., Williams, R.G., Torres-Valdes, S., Woodward, E.M.S., Landolfi, A., Pan, X., Sanders, R., Achterberg, E.P., 2008. Phosphorus cycling in the North and South Atlantic Ocean subtropical gyres. Nat. Geosci. 1, 439–443. doi: 10.1038/ngeo232.

Moore, L.R., Ostrowski, M., Scanlan, D.J., Feren, K., Sweetsir, T., 2005. Ecotypic variation in phosphorus acquisition mechanisms within marine picocyanobacteria. Aquat. Microb. Ecol. 39, 257–269.

Morel, A., Gentili, B., Claustre, H., Babin, M., Bricaud, A., Ras, J., Tieche, F., 2007. Optical properties of the "clearest" natural waters. Limnol. Oceanogr. 52, 217–229. http://dx.doi.org/10.4319/lo.2007.52.1.0217.

Moutin, T., Karl, D.M., Duhamel, S., Rimmelin, P., Raimbault, P., Van Mooy, B.A.S., Claustre, H., 2008. Phosphate availability and the ultimate control of new nitrogen input by nitrogen fixation in the tropical Pacific Ocean. Biogeosciences 5, 95–109.

Moutin, T., Van Den Broeck, N., Beker, B., Dupouy, C., Rimmelin, P., Le Bouteiller, A., 2005. Phosphate availability controls *Trichodesmium* spp. biomass in the SW Pacific Ocean. Mar. Ecol. Prog. Ser. 297, 15–21.

Nawrocki, M.P., Karl, D.M., 1989. Dissolved ATP turnover in the Bransfield Strait, Antarctica during a spring bloom. Mar. Ecol. Prog. Ser. 57, 35–44.

Orchard, E.D., Ammerman, J.W., Lomas, M.W., Dyhrman, S.T., 2010. Dissolved inorganic and organic phosphorus uptake in *Trichodesmium* and the microbial community: the importance of phosphorus ester in the Sargasso Sea. Limnol. Oceanogr. 55, 1390–1399.

Paytan, A., McLaughlin, K., 2007. The oceanic phosphorus cycle. Chem. Rev. 107, 563–576.

Raimbault, P., Garcia, N., Cerutti, F., 2008. Distribution of inorganic and organic nutrients in the South Pacific Ocean – evidence for long-term accumulation of organic matter in nitrogen-depleted waters. Biogeosciences 5, 281–298.

Repeta, D.J., Ferron, S., Sosa, O.A., Johnson, C.G., Repeta, L.D., Acker, M., DeLong, E.F., Karl, D.M., 2016. Marine methane paradox explained by bacterial degradation of dissolved organic matter. Nat. Geosci. 9, 884–887.

Rii, Y.M., Duhamel, S., Bidigare, R.R., Karl, D.M., Repeta, D., Church, M.J., 2016. Diversity and productivity of photosynthetic picoeukaryotes in biogeochemically distinct regions of the South East Pacific Ocean. Limnol. Oceanogr. 61, 806–824. http://dx.doi.org/10.1002/lno.10255.

Ruttenberg, K.C., Dyhrman, S.T., 2012. Dissolved organic phosphorus production during simulated phytoplankton blooms in a coastal upwelling system. Front. Microbiol. 3, 274.

Scanlan, D.J., Ostrowski, M., Mazard, S., Dufresne, A., Garczarek, L., Hess, W.R., Post, A.F., Hagemann, M., Paulsen, I., Partensky, F., 2009. Ecological genomics of marine picocyanobacteria. Microbiol. Mol. Biol. Rev. 73, 249–299. http://dx.doi.org/10.1128/MMBR.00035-08.

Stramma, L., Peterson, R.G., Tomczak, M., 1995. The south Pacific current. J. Phys. Oceanogr. 25, 77–91.

Strickland, J., Parsons, T., 1972. A Practical Handbook of Seawater Analysis, vol. 167, Ottawa.

Sverdrup, H.U., Johnson, M.W., Fleming, R.H., 1942. The oceans: their Physics, Chemistry, and General Biology. Prentice-Hall Inc., New York.

Tedetti, M., Sempr, R., Vasilkov, A., Charrire, B., Nrini, D., Miller, W.L., Kawamura, K., Raimbault, P., 2007. High penetration of ultraviolet radiation in the south east Pacific waters. Geophys. Res. Lett. 34, L12610. http://dx.doi.org/10.1029/2007GL029823.

Worden, A.Z., Nolan, J.K., Palenik, B., 2004. Assessing the dynamics and ecology of marine picophytoplankton: the importance of the eukaryotic component. Limnol. Oceanogr. 49, 168–179.

Young, C., Ingall, E., 2010. Marine dissolved organic phosphorus composition: insights from samples recovered using combined electrodialysis/reverse osmosis. Aquat. Geochem. 16, 563–574. http://dx.doi.org/10.1007/s10498-009-9087-y.